

Explicit Estimation of Magnitude and Phase Spectra in Parallel for High-Quality Speech Enhancement

Ye-Xin Lu, Yang Ai, *Member, IEEE*, Zhen-Hua Ling, *Senior Member, IEEE*

Abstract—Phase information has a significant impact on speech perceptual quality and intelligibility. However, existing speech enhancement methods encounter limitations in explicit phase estimation due to the non-structural nature and wrapping characteristics of the phase, leading to a bottleneck in enhanced speech quality. To overcome the above issue, in this paper, we proposed MP-SENet, a novel Speech Enhancement Network which explicitly enhances Magnitude and Phase spectra in parallel. The proposed MP-SENet adopts a codec architecture in which the encoder and decoder are bridged by time-frequency Transformers along both time and frequency dimensions. The encoder aims to encode time-frequency representations derived from the input distorted magnitude and phase spectra. The decoder comprises dual-stream magnitude and phase decoders, directly enhancing magnitude and wrapped phase spectra by incorporating a magnitude estimation architecture and a phase parallel estimation architecture, respectively. To train the MP-SENet model effectively, we define multi-level loss functions, including mean square error and perceptual metric loss of magnitude spectra, anti-wrapping loss of phase spectra, as well as mean square error and consistency loss of short-time complex spectra. Experimental results demonstrate that our proposed MP-SENet excels in high-quality speech enhancement across multiple tasks, including speech denoising, dereverberation, and bandwidth extension. Compared to existing phase-aware speech enhancement methods, it successfully avoids the bidirectional compensation effect between the magnitude and phase, leading to a better harmonic restoration. Notably, for the speech denoising task, the MP-SENet yields a state-of-the-art performance with a PESQ of 3.60 on the public VoiceBank+DEMAND dataset.

Index Terms—Speech enhancement, encoder-decoder, magnitude prediction, phase prediction, explicit estimation.

I. INTRODUCTION

IN real-life scenarios, speech signals captured by devices are inevitably distorted by intrusive noises and their self-reflections from the surfaces of surrounding objects. For the bandwidth-limited scenario, when these captured signals are transmitted between narrowband communication devices, only their low-frequency components are typically preserved. These issues immensely degrade the performances of automatic speech recognition, hearing aids, and telecommunication systems [2], [3]. In this regard, speech enhancement (SE) aims to improve the intelligibility and overall perceptual quality of distorted speech signals. With the development of deep

learning and deep neural network (DNN), numerous DNN-based SE methods have been proposed to specifically address one or more of these issues, with the aim of recovering the original speech signals from the distorted ones.

For speech signal processing, the phase information determines the temporal and spectral characteristics of the speech signal, exerting a substantial impact on the naturalness and intelligibility of the reconstructed speech. In convolutional SE methods, restoring phase information has long been underestimated, with distorted phase being used as an optimal estimator of the original phase [4]. However, recent studies demonstrated the noteworthy contribution of precise knowledge of the phase spectrum to speech quality [5]. The phase information ensures coherence across time frames and between adjacent frequency bins in the time-frequency (TF) domain. Accurately preserving it during enhancement helps maintain the temporal characteristics and harmonic structures of the original speech.

Despite the significance of phase reconstruction in SE tasks, existing SE methods still face challenges in precisely modeling and optimizing the phase due to its non-structural nature and wrapping characteristics. Time-domain SE methods [6]–[11], which utilized neural networks to learn the mapping from distorted waveforms to original ones, implicitly restored phase information without direct phase modeling. Unfortunately, this category of methods still suffered from bottlenecks in enhanced speech quality and showed inefficiency due to the direct generation of high-resolution waveforms. For the TF-domain phase-aware SE methods, some of them focused on the enhancement of the short-time complex spectrum, which implicitly recovered both the magnitude and phase spectra within the complex-valued spectral domain [12]–[15]. However, in the absence of explicit magnitude and phase optimizations, the bidirectional compensation effect [16] between magnitude and phase would emerge, leading to imprecise magnitude and phase estimations, consequently constraining the quality of the reconstructed speech. Recently, several advancements in the form of multi-stage decoupling-style methods have been proposed which first explicitly enhanced the magnitude spectrum and subsequently conducted complex spectrum refinement to implicitly enhance the phase spectrum [17]–[20]. While the multi-stage decoupling-style methods successfully alleviated the compensation effect from magnitude to phase with explicit magnitude optimization, they were still plagued by implicit phase estimation, which would cause damage to the harmonic structure of the enhanced speech and limit the enhanced speech quality. Overall, existing SE methods were still unable to precisely estimate the original phase spectrum, leaving room for improvements in speech perceptual quality

The authors are with the National Engineering Research Center of Speech and Language Information Processing, University of Science and Technology of China, Hefei 230027, China (e-mail: yxlu0102@mail.ustc.edu.cn; yangai@ustc.edu.cn; zhling@ustc.edu.cn).

This work was supported by the Fundamental Research Funds for the Central Universities under Grant WK2100000033.

This work is the extended version of our conference paper [1] published at Interspeech 2023.

and intelligibility.

Therefore, we introduce MP-SENet, a TF-domain monaural SE model that performs parallel estimations of magnitude and phase spectra. The MP-SENet adopts a codec architecture, connecting the encoder and decoder with Transformers [21] across both time and frequency dimensions, enabling the capture of alternating time and frequency dependencies. The encoder encodes the input distorted magnitude and wrapped phase spectra into TF-domain representations for subsequent decoding. The parallel magnitude decoder and phase decoder estimate the original magnitude and phase spectra, respectively, and the enhanced speech waveforms are finally reconstructed using inverse short-time Fourier transform (ISTFT). To realize explicit phase enhancement, we follow our previous work [22] to utilize the parallel estimation architecture and anti-wrapping loss to model and optimize the phase spectra, respectively. Additionally, we also utilize mean square error (MSE) loss defined on the magnitude spectra, MSE loss and spectral consistency loss defined on the short-time complex spectra to help train the MP-SENet model effectively. Furthermore, to address the incomplete correlation between these objective losses and human auditory perception, we incorporate a metric discriminator [23] to further enhance the speech perceptual quality. Experimental results demonstrate that MP-SENet surpasses state-of-the-art (SOTA) SE methods across speech denoising, dereverberation, and bandwidth extension tasks in speech quality by explicitly modeling and optimizing both magnitude and phase spectra.

The main contribution of this work lies in the direct enhancement of the wrapped phase spectra, which mitigates the bidirectional compensation effect between magnitude and phase spectra and results in excellent harmonic restoration. Our proposed MP-SENet exhibits the ability to handle three distinct SE tasks, i.e., speech denoising, dereverberation, and bandwidth extension, showcasing its generalization capability across different SE tasks.

The rest of this paper is organized as follows. Section II briefly reviews several phase-aware DNN-based SE methods and the relevant backgrounds of three aforementioned SE tasks. In Section III, we give details of our proposed MP-SENet framework. The experimental setup is presented in Section IV, while Section V gives the results and analysis. Finally, we give conclusions in Section VI.

II. RELATED WORK

A. Phase-aware SE Methods

In traditional SE methods, only the magnitude spectrum was enhanced and then combined with the distorted phase spectrum to reconstruct the enhanced speech using ISTFT [24]–[27]. Upon recognizing the importance of phase reconstruction in improving the quality of enhanced speech, plenty of phase-aware SE methods have been proposed to recover phase information from distorted speech or spectral features (e.g., magnitude spectrum and mel-spectrogram). These methods mainly operate in the TF domain and can be broadly categorized as follows.

The first category of phase-aware SE methods enhances the phase spectrum indirectly by manipulating the complex

spectrum. The most common method is complex spectrum masking, which predicts a complex-valued mask applied to the real and imaginary parts of the distorted short-time complex spectrum, implicitly enhancing both the magnitude and phase spectra [13], [14], [28]. Although this category of approach does not involve direct modeling and optimization of magnitude and phase, accurate phase estimation is inherently challenging. As a result, the magnitude of the estimated complex spectrum would tend to compensate for inaccuracies in phase estimation [16], leading to damages to both the magnitude and phase of the reconstructed speech, significantly impacting the speech perceptual quality and intelligibility.

Another category of phase-aware SE methods decomposes the complex spectrum estimation problem into two sub-stages, where the magnitude estimation is involved in the first stage, followed by complex-spectrum refinement with residual learning in the second stage. Taking the most representative CMGAN [19] as an example, it involves the use of magnitude spectrum masking and complex spectrum mapping. The overall architecture of CMGAN is a convolution-augmented Transformer (Conformer) [29] based codec. The encoder encodes the magnitude and complex spectral information using two-stage Conformer blocks to capture both time and frequency dependencies. The decoder consists of a magnitude mask decoder branch for preliminary enhancement of the magnitude spectrum and a complex refinement branch to improve the accuracy of magnitude estimation as well as implicitly enhance the phase spectrum. This category of methods introduces explicit modeling and optimization of magnitude on the basis of complex spectral enhancement methods, effectively alleviating the compensation effect from magnitude to phase. However, the problem of inaccurate phase estimation still persists, leading to damage in the harmonic structure, ultimately limiting the quality of the enhanced speech.

The last category of phase-aware SE methods incorporates a dual-stream architecture to separately predict magnitude and phase. For instance, PHASEN [30] proposes a two-stream network with bidirectional information communication for efficient phase prediction. These two streams are designed to communicate with each other for information exchange so that the predicted magnitude can guide the prediction of phase. Since phase correlation between harmonics can be used for speech phase reconstruction [31], [32], PHASEN also designs a learnable frequency transformation matrix to implicitly learn a pattern that is consistent with harmonic correlation. With explicit phase modeling and the ability to capture harmonic correlation, PHASEN can handle detailed phase patterns and utilize harmonic patterns, achieving a promising SE performance. However, it only implicitly optimizes the phase in the complex-valued spectral domain, making it challenging to achieve precise phase estimation. Inaccurate phase estimation would still do harm to the reconstructed speech waveforms, damage their harmonic structures, and affect the enhanced speech quality.

In summary, existing phase-aware SE methods are still constrained by imprecise phase enhancement. This limitation can adversely affect the quality of enhanced speech and disrupt harmonic structures. Thus, there is scope for improvement

in terms of speech perceptual quality and intelligibility by undertaking explicit phase modeling and optimization in TF-domain SE methods.

B. Speech Enhancement Tasks

The main focus of this paper is on speech denoising, dereverberation, and bandwidth extension in SE tasks. In this section, we will sequentially introduce the backgrounds and relevant methods for these three tasks.

1) *Speech denoising*: Speech denoising aims to remove the additive noise signal from the noisy speech signal. Classic signal-processing-based speech denoising methods include spectral subtraction [33], Wiener filtering [34], statistical model-based methods [35], subspace algorithms [36], [37], etc. These traditional methods often require prior information and face challenges in dealing with non-stationary noise. With the renaissance of deep learning, DNN-based denoising methods demonstrate strong noise suppression capabilities for non-stationary noise and achieve better SE performance. Existing DNN-based denoising methods can be classified into two categories, i.e., time-domain methods and TF-domain methods.

Time-domain denoising methods aim to predict clean speech waveforms directly from noisy ones without any frequency transformation. One of the most notable methods in this category is SEGAN [6], which employs generative adversarial networks (GANs) to learn the mapping from noisy speech waveforms to clean ones at the waveform level. While this category of methods successfully avoids the phase estimation problem encountered in TF-domain methods, they sacrifice the ability to capture speech phonetics in the frequency domain. Consequently, this trade-off can lead to artifacts in enhanced speech waveforms. As a result, the performance of time-domain denoising methods is generally considered inferior to that of TF-domain methods.

TF-domain denoising methods are predominantly based on spectral mapping or masking. Mapping-based methods map the spectral representations of degraded speech to those of clean speech [24], [26], [38]. Masking-based methods initially enhance the magnitude spectrum using ideal binary mask (IBM) [39], ideal ratio mask (IRM) [40], [41], and spectral magnitude mask (SMM) [42] to selectively attenuate the noise components based on the mask values. Recognizing the significance of phase information, phase-sensitive mask (PSM) [43] and complex ideal ratio mask (cIRM) [44] were proposed based on SMM and IRM, respectively. PSM remains a real-valued mask with additional phase estimation, allowing the estimated magnitude to compensate for the noisy phase, while cIRM is a complex-valued mask used to directly enhance the complex spectrum. In addition, the multi-style decoupling-style methods we mentioned in the previous section also belong to this category of methods. They combine the advantages of mapping-based and masking-based methods, achieving precise magnitude enhancement and implicit phase enhancement.

2) *Dereverberation*: Speech dereverberation aims to mitigate the convolutive effects or reflections caused by the surfaces of surrounding objects, which result in smearing effects across the time and frequency domains of the original speech

waveforms. The quantity and intensity of these reflections are influenced by factors such as room size, surface properties, and microphone distance. These reflections can be effectively modeled using the room impulse response (RIR) filter.

In the early research, signal processing techniques were employed to eliminate the convolutive effects caused by reverberation via statistical modeling of the RIRs. For instance, the weighted prediction error (WPE) algorithm [45], [46] employs long-term linear prediction to estimate the impact of RIRs on reverberant speech waveforms, which assumes that the early reflections of RIRs, along with the direct path, are crucial for improved recognition, while late reflections are considered diffused and detrimental to speech intelligibility.

DNN-based speech dereverberation methods are generally similar to the approaches used in denoising tasks, and there are models capable of simultaneously handling both denoising and dereverberation tasks. Since reverberation manifests as smearing effects in the TF-domain spectrum, IBM [47] and IRM [48], [49] based methods predict masks applied to the reverberant magnitude spectra, combined with the unprocessed reverberant phase spectra, to reconstruct the anechoic speech waveforms. Following the speech denoising task, cIRM is further employed based on the IRM to implicitly reconstruct the phase [28], [50]. Furthermore, there are also some mapping-based methods that have achieved effective dereverberation performance [15], [51], [52].

3) *Bandwidth extension*: Bandwidth extension aims to supplement the truncated frequency bandwidth and enhance the quality and intelligibility of the speech signal. Therefore, it can also be regarded as a SE task. Unlike speech denoising or dereverberation methods that remove noise or reverberation components from the spectrum while preserving a clean spectrum, the bandwidth extension methods predict the high-frequency components from the narrowband spectrum in the TF domain to obtain a wideband spectrum. Compared to traditional signal-processing-based bandwidth extension methods which often result in overly smoothed spectra [53], recent DNN-based methods have shown superior performance.

In the DNN-based bandwidth extension methods, early studies predominantly focused on the extension of the magnitude spectrum while the upper band phase spectrum was obtained through the replication [54] or mirror inversion [55] of the narrowband phase spectrum. AudioUNet [11] directly generates high-resolution speech waveforms from low-resolution ones using an autoencoder architecture, avoiding the separate estimation of the phase spectrum. Building upon AudioUNets, TFNet [56] combines both time-domain and frequency-domain information by using two AudioUNet-based branches. One branch takes the low-resolution waveform as input, while the other takes the narrowband magnitude spectrum. A spectral fusion module is used to obtain the final wideband output, and the prediction of the wideband phase spectrum is derived from the high-resolution waveform output of the time-domain branch. Wang *et al.* [57] takes advantage of information from both time and frequency domains by using an autoencoder model for time-domain super-resolution and optimizing it using cross-domain loss.

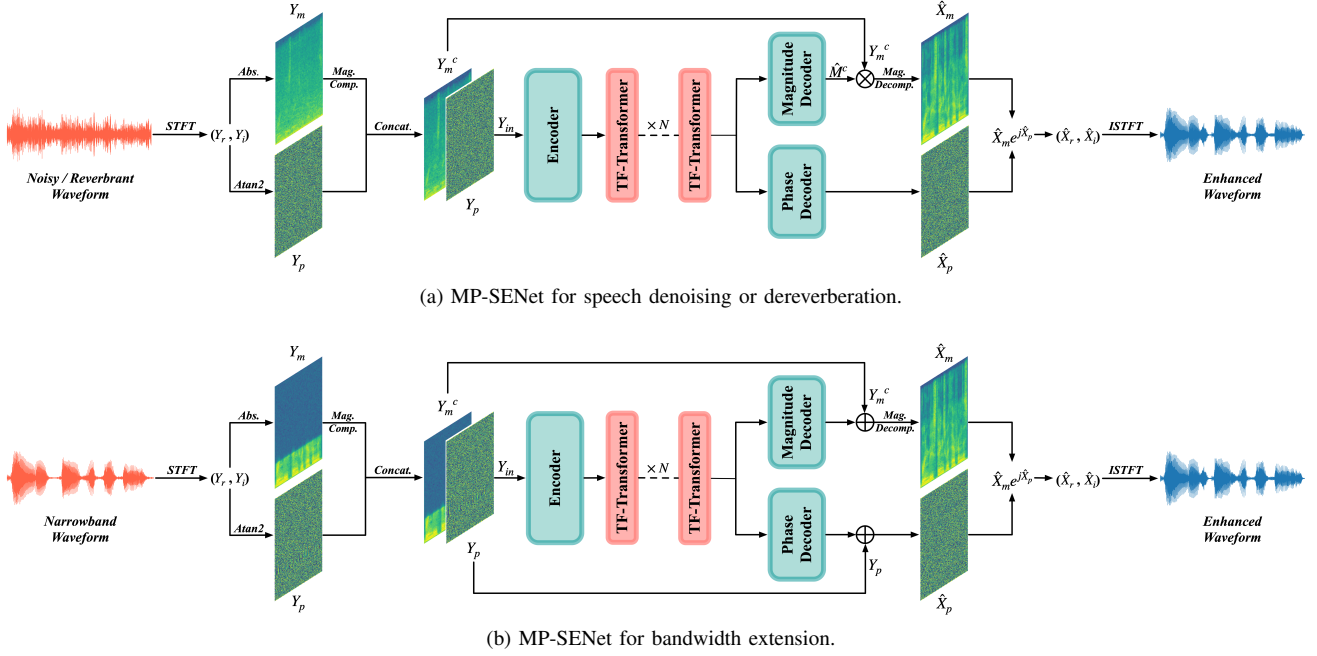


Fig. 1. Overall structure of the proposed MP-SENet for (a) denoising/dereverberation tasks and (b) bandwidth extension task. The “Abs.” and “Atan2” represent the absolute value function and two-argument arctangent function used to calculate magnitude and phase spectra, respectively. The “Concat.,” “Mag. Comp.” and “Mag. Decom.” denote the spectral concatenation, magnitude compression and decompression operations, respectively.

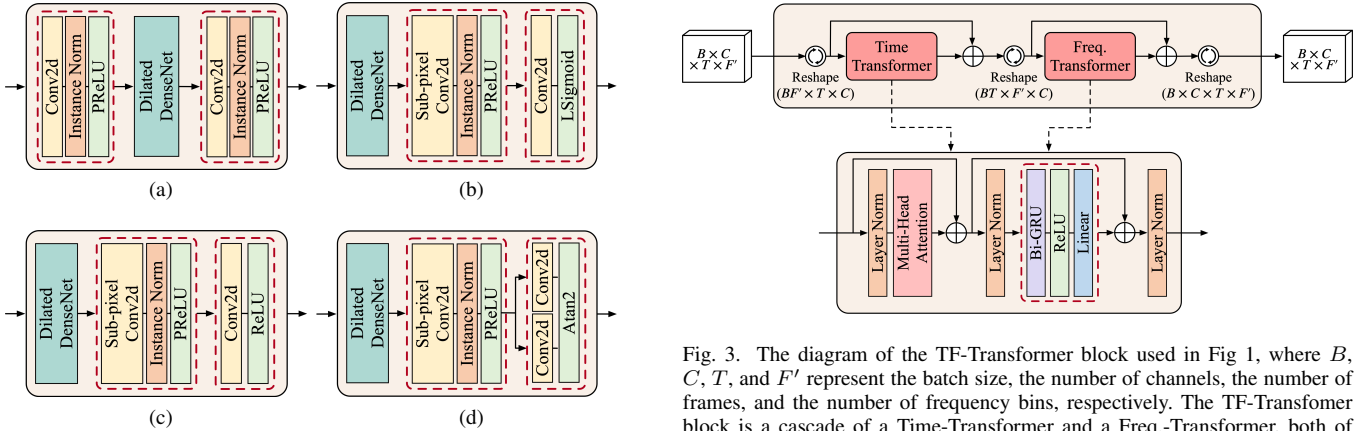


Fig. 2. The architectural details of the (a) encoder, (b) magnitude decoder for speech denoising or dereverberation, (c) magnitude decoder for bandwidth extension, and (d) phase decoder used in Fig. 1.

III. METHODOLOGY

A. Model Structure

An overview of the model structure of the proposed MP-SENet is illustrated in Fig. 1. Due to distinct prediction objectives for denoising or dereverberation tasks compared to bandwidth extension, we have made specific adjustments to the magnitude decoder structure and generation process of our MP-SENet for these two categories of tasks, as depicted in Fig. 1a and Fig. 1b, respectively.

Generally, the MP-SENet employs a codec architecture to enhance the distorted speech waveform $\mathbf{y} \in \mathbb{R}^L$ and recover the original speech waveform $\mathbf{x} \in \mathbb{R}^L$ in the TF domain, where L represents the length of the waveform. To begin, we

extract the magnitude spectrum $\mathbf{Y}_m \in \mathbb{R}^{T \times F}$ and the wrapped phase spectrum $\mathbf{Y}_p \in \mathbb{R}^{T \times F}$ from \mathbf{y} using short-time Fourier transform (STFT), where T and F denote the total number of frames and frequency bins, respectively. Before feeding them to the encoder, we follow [30] to apply the power-law compression on \mathbf{Y}_m and get a compressed magnitude spectrum $\mathbf{Y}_m^c \in \mathbb{R}^{T \times F}$, where c is the compression factor and is set to 0.3 in our experiments. The input feature $\mathbf{Y}_{in} \in \mathbb{R}^{T \times F \times 2}$ of MP-SENet is the concatenation of the \mathbf{Y}_m^c and \mathbf{Y}_p . The encoder encodes \mathbf{Y}_{in} into a compressed TF-domain representation, and subsequently, the TF-domain representation is processed by N time-frequency transformer (TF-Transformer) blocks to alternately capture time and frequency dependencies. In the final stages, the parallel magnitude decoder and phase decoder predict the original magnitude spectrum $\hat{\mathbf{X}}_m \in \mathbb{R}^{T \times F}$

and wrapped phase spectrum $\hat{\mathbf{X}}_p \in \mathbb{R}^{T \times F}$ from the TF-domain representation, respectively. Subsequently, the enhanced waveform \hat{x} is reconstructed through ISTFT. Further insight into the encoder, TF-Transformer block, magnitude decoder, and phase decoder is elaborated below.

1) *Encoder*: As illustrated in Fig. 1, the encoder transforms the input feature \mathbf{Y}_{in} into a TF-domain representation with C channels, T temporal dimensions, and $F' = F/2$ frequency dimensions. The architectural detail of the encoder is depicted in Fig. 2a, which is a cascade of a convolutional block, a dilated DenseNet [58], and another convolutional block. Each convolutional block comprises a 2D convolutional layer, an instance normalization [59], and a parametric rectified linear unit (PReLU) activation [60]. The first convolutional block increases the channel numbers of the TF-domain representation to C , and the second convolutional block halves the feature dimension F to F' to reduce the subsequent computational complexity in the TF-Transformer blocks. The dilated DenseNet utilizes four convolutional layers with dilation sizes of 1, 2, 4, and 8 to extend the receptive field along the time axis, facilitating context aggregation at different resolutions. Additionally, it incorporates dense connections at each convolutional layer, connecting to all previous layers. This not only helps prevent the vanishing gradient problem but also enhances the parameter efficiency of the network.

2) *TF-Transformer*: The dual-path attention-based structure [18], [20], [61]–[64] has demonstrated remarkable performance in SE tasks, primarily due to its ability to capture both time and frequency dependencies. Compared to our previous conference paper [1], this study replaces the Conformers with Transformers and presents the TF-Transformer block, which can sequentially capture long-range correlations exhibited in the temporal and spectral domains. As illustrated in Fig. 3, the TF-Transformer block takes an intermediate TF-domain representation as input, with a shape of $B \times C \times T \times F'$, where B denotes the batch size. Initially, this representation is reshaped to $BF' \times T \times C$ and passed through the Time-Transformer layer to capture temporal dependencies. Subsequently, it is reshaped to $BT \times F' \times C$ and fed into the Frequency-Transformer layer to capture frequency dependencies. Finally, the intermediate TF-domain representation is reshaped back to $B \times C \times T \times F'$ and output to the remaining three TF-Transformer blocks.

For each TF-Transformer block, both the Time-Transformer layer and the Frequency-Transformer layer share the same architecture, which is a gated recurrent unit (GRU) based Transformer [62]. The GRU-based transformer consists of a multi-head self-attention (MHSA) [21] and a GRU-based position-wise feed-forward network (FFN), augmented with layer normalizations [65] and residual connections. The MHSA with M heads enables the model to collectively focus on the global information from different representation subspaces at various positions. The GRU-based position-wise FFN comprises a bidirectional GRU (Bi-GRU) layer, a rectified linear unit (ReLU) activation [66], and a linear layer to learn the local information [67].

3) *Magnitude decoder*: For speech denoising or dereverberation, as illustrated in Fig 1a, the magnitude decoder predicts a compressed magnitude mask $\hat{\mathbf{M}}^c \in \mathbb{R}^{T \times F}$ from the TF-

domain representation and multiplies it with the compressed distorted magnitude spectrum \mathbf{Y}_m^c to obtain the enhanced magnitude spectrum $\hat{\mathbf{X}}_m$ as follows:

$$\hat{\mathbf{X}}_m = (\mathbf{Y}_m^c \odot \hat{\mathbf{M}}^c)^{\frac{1}{c}}, \quad (1)$$

where \odot denotes the element-wise multiplication operator. For bandwidth extension, as illustrated in Fig 1b, the magnitude decoder predicts a compressed high-frequency magnitude spectrum from the TF-domain representation and adds it to the compressed low-frequency magnitude spectrum \mathbf{Y}_m^c to obtain the wideband magnitude spectrum $\hat{\mathbf{X}}_m$.

The architectural details of magnitude decoders are depicted in Fig. 2b and Fig. 2c. Both the magnitude decoders comprise a dilated DenseNet, a deconvolutional block, and a magnitude estimation architecture. The deconvolutional block is composed of a 2D sub-pixel convolutional layer [68], an instance normalization, and a PReLU activation. The sub-pixel convolutional layer is used to upsample the frequency dimensions of the TF-domain representation back to F while avoiding checkerboard artifacts compared to transposed convolution. The magnitude estimation architecture comprises a 2D convolutional layer and an activation function. The convolutional layer is used to reduce the output channel numbers of the deconvolutional block to 1. For speech denoising or dereverberation, as depicted in Fig. 2b, we use the learnable sigmoid (LSigmoid) function [69] to estimate a boundary magnitude mask $\hat{\mathbf{M}}^c$:

$$\text{LSigmoid}(t) = \frac{\beta}{1 + e^{1-\alpha t}}, \quad (2)$$

where β is set to 2.0, and $\alpha \in \mathbb{R}^F$ is a trainable frequency-related parameter, which enables the model to adaptively adjust the shape of the activation function across frequency bands. For bandwidth extension, as depicted in Fig. 2c, we replace the LSigmoid activation with ReLU to predict the unbounded high-frequency magnitude spectrum.

4) *Phase decoder*: For speech denoising and dereverberation, as illustrated in Fig 1a, the phase decoder directly predicts the enhanced wrapped phase spectrum $\hat{\mathbf{X}}_p$ from the TF-domain representation. For bandwidth extension, as illustrated in Fig 1b, we observed that directly predicting the wideband phase spectrum from the narrowband one would introduce horizontal lines in the silent area of the high-frequency phase spectrum, causing artifacts such as buzzing noise in the generated speech. Therefore, we employ the phase decoder to output the residual wrapped phase spectrum, which represents the difference between the narrowband phase spectrum and the wideband phase spectrum, effectively alleviating the presence of buzzing noise. And the final extended wideband phase spectrum $\hat{\mathbf{X}}_p$ is the addition of the narrowband phase spectrum $\hat{\mathbf{Y}}_p$ and the predicted residual phase spectrum.

The architectural detail of the phase decoder is depicted in Fig. 2d. To address the challenges posed by the non-structural nature and wrapping characteristics of the phase, we follow our previous work [22] and incorporate the parallel estimation architecture after a dilated DenseNet and a deconvolutional block in the phase decoder. For speech denoising or dereverberation, the parallel estimation architecture first adopts two

parallel 2D convolutional layers to output the pseudo-real part component $\hat{\mathbf{X}}_p^{(r)} \in \mathbb{R}^{T \times F}$ and pseudo-imaginary part component $\hat{\mathbf{X}}_p^{(i)} \in \mathbb{R}^{T \times F}$, and then activates these two components to obtain the enhanced wrapped phase spectrum $\hat{\mathbf{X}}_p$ using the two-argument arctangent (Atan2) function, represented as follows,

$$\hat{\mathbf{X}}_p = \arctan \left(\frac{\hat{\mathbf{X}}_p^{(i)}}{\hat{\mathbf{X}}_p^{(r)}} \right) - \frac{\pi}{2} \cdot \text{Sgn}^*(\hat{\mathbf{X}}_p^{(i)}) \cdot [\text{Sgn}^*(\hat{\mathbf{X}}_p^{(r)}) - 1], \quad (3)$$

where $\text{Sgn}^*(t)$ is a redefined function which equals to 1 when $t \geq 0$, and equals to -1 when $t < 0$. For bandwidth extension, the parallel estimation architecture outputs the residual wrapped phase spectrum.

B. Training Criteria

As illustrated in Fig. 4, We define multi-level loss functions on the magnitude spectra, phase spectra, and short-time complex spectra to jointly train the proposed MP-SENet. These loss functions are described as follows.

1) *Loss functions defined on magnitude spectra:* We first define loss functions on the magnitude spectra to explicitly optimize the magnitude and further improve the magnitude-based speech perceptual metrics, including:

- **MSE Loss of Magnitude Spectra:** We define the MSE loss $\mathcal{L}_{\text{MSE}_{\text{Mag}}}$ between the original and enhanced magnitude spectra \mathbf{X}_m and $\hat{\mathbf{X}}_m$ to explicitly optimize the magnitude spectrum:

$$\mathcal{L}_{\text{MSE}_{\text{Mag}}} = \mathbb{E}_{\mathbf{X}_m, \hat{\mathbf{X}}_m} [\|\mathbf{X}_m - \hat{\mathbf{X}}_m\|_2^2]. \quad (4)$$

- **Metric Loss of Magnitude Spectra:** The primary goal of SE is to improve the quality and intelligibility of distorted speech considering human perception [70]. However, specific objective metrics associated with human perception, such as the perceptual evaluation of speech quality (PESQ) [71] and short-time objective intelligibility (STOI) [72], are non-differentiable. Thus they cannot be directly used as loss functions. To overcome this issue, MetriGAN [23] introduces a metric discriminator as a learned surrogate of the evaluation metrics. The metric discriminator iteratively estimates a surrogate loss that approaches the sophisticated metric surface, enabling the SE model to leverage this surrogate to determine the optimization direction toward achieving improved speech perceptual quality.

We here adopt the metric discriminator from [19] for adversarial training, which uses magnitude spectra as input conditions. For training the discriminator, we choose the PESQ as the target objective metric. We define the discriminator loss \mathcal{L}_D which conducts the discriminator to output the maximum normalized PESQ scores (=1) with pairs of reference magnitude spectra as input and output the corresponding normalized PESQ scores with pairs of reference and enhanced magnitude spectra as input, respectively. With this discriminator, we subsequently define the metric loss $\mathcal{L}_{\text{Metric}}$ to guide the model training in generating speech waveforms whose magnitude spectra

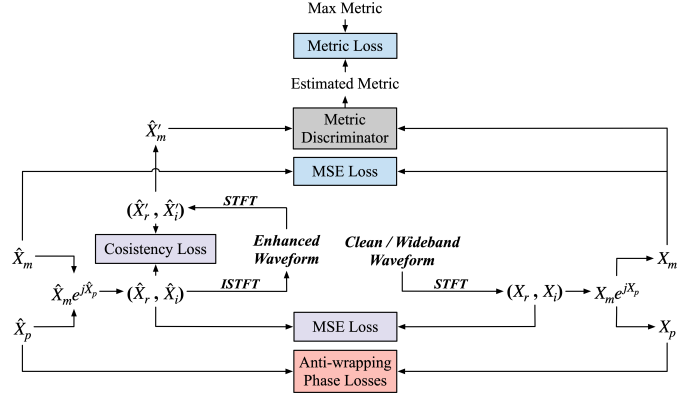


Fig. 4. Training criteria of the proposed MP-SENet. The losses with the blue, red, and purple background represent they are defined on the magnitude spectra, phase spectra, and short-time complex spectra, respectively.

correspond to high PESQ scores. The discriminator loss \mathcal{L}_D and the corresponding generated metric loss $\mathcal{L}_{\text{Metric}}$ are described as follows:

$$\mathcal{L}_D = \mathbb{E}_{\mathbf{X}_m} [\|D(\mathbf{X}_m, \mathbf{X}_m) - 1\|_2^2] + \mathbb{E}_{\mathbf{X}_m, \hat{\mathbf{X}}'_m} [\|D(\mathbf{X}_m, \hat{\mathbf{X}}'_m) - Q_{\text{PESQ}}\|_2^2], \quad (5)$$

$$\mathcal{L}_{\text{Metric}} = \mathbb{E}_{\mathbf{X}_m, \hat{\mathbf{X}}'_m} [\|D(\mathbf{X}_m, \hat{\mathbf{X}}'_m) - 1\|_2^2], \quad (6)$$

where D denotes the discriminator and $Q_{\text{PESQ}} \in [0, 1]$ denotes the scaled PESQ score.

The total loss defined on magnitude spectra is the linear combination of the MSE loss and metric loss:

$$\mathcal{L}_{\text{Mag}} = \gamma_1 \mathcal{L}_{\text{MSE}_{\text{Mag}}} + \gamma_2 \mathcal{L}_{\text{Metric}}. \quad (7)$$

where γ_1 and γ_2 are hyperparameters.

2) *Loss functions defined on phase spectra:* To explicitly optimize the phase spectrum, considering the phase wrapping property, the absolute distance between the original and enhanced phase spectra \mathbf{X}_p and $\hat{\mathbf{X}}_p$ may not accurately reflect their actual distance, revealing the inappropriateness of conventional phase losses (e.g., absolute L^p distance) for phase optimization. Thus, we utilize the anti-wrapping function we proposed in [22] to prevent error expansion caused by phase wrapping, which is defined as:

$$f_{\text{AW}}(t) = |t - 2\pi \cdot \text{round}(\frac{t}{2\pi})|, t \in \mathbb{R}. \quad (8)$$

On the basis of the anti-wrapping function, we here define three **anti-wrapping phase losses** to improve the precision and continuity of the estimated phase spectra, including:

- **Instantaneous Phase Loss:** The instantaneous phase (IP) loss \mathcal{L}_{IP} is the mean absolute error (MAE) between the anti-wrapped original and enhanced IP spectra, i.e.,

$$\mathcal{L}_{\text{IP}} = \mathbb{E}_{\mathbf{X}_p, \hat{\mathbf{X}}_p} [\|f_{\text{AW}}(\mathbf{X}_p - \hat{\mathbf{X}}_p)\|_1]. \quad (9)$$

- **Group Delay Loss:** The group delay (GD) loss \mathcal{L}_{GD} is the MAE between the anti-wrapped original and enhanced GD spectra, i.e.,

$$\mathcal{L}_{\text{GD}} = \mathbb{E}_{\Delta_{\text{DF}}(\mathbf{X}_p, \hat{\mathbf{X}}_p)} [\|f_{\text{AW}}(\Delta_{\text{DF}}(\mathbf{X}_p - \hat{\mathbf{X}}_p))\|_1], \quad (10)$$

where Δ_{DF} represents the differential operator along the frequency axis.

- **Instantaneous Angular Frequency Loss:** The instantaneous angular frequency (IAF) loss \mathcal{L}_{IAF} is the MAE between the anti-wrapped original and enhanced IAF spectra, i.e.,

$$\mathcal{L}_{\text{IAF}} = \mathbb{E}_{\Delta_{DT}(\mathbf{X}_p, \hat{\mathbf{X}}_p)} [\|f_{\text{AW}}(\Delta_{DT}(\mathbf{X}_p - \hat{\mathbf{X}}_p))\|_1], \quad (11)$$

where Δ_{DT} represents the differential operator along the temporal axis.

The total loss defined on phase spectra is the sum of IP loss, GD loss, and IAF loss:

$$\mathcal{L}_{\text{Pha.}} = \mathcal{L}_{\text{IP}} + \mathcal{L}_{\text{GD}} + \mathcal{L}_{\text{IAF}}. \quad (12)$$

3) *Loss functions defined on complex spectra:* We finally define loss functions on the short-time complex spectra to implicitly enhance both the magnitude and phase spectra as well as guarantee the consistency of the complex spectra reconstructed through ISTFT, including:

- **MSE loss of Complex Spectra:** To further optimize the magnitude and phase spectra within the complex domain, we define the MSE loss $\mathcal{L}_{\text{MSECom.}}$ between the real and imaginary parts of the original and enhanced complex spectrum $(\mathbf{X}_r, \mathbf{X}_i)$ and $(\hat{\mathbf{X}}_r, \hat{\mathbf{X}}_i)$ as follows:

$$\mathcal{L}_{\text{MSECom.}} = \mathbb{E}_{\mathbf{X}_r, \hat{\mathbf{X}}_r} [\|\mathbf{X}_r - \hat{\mathbf{X}}_r\|_2^2] + \mathbb{E}_{\mathbf{X}_i, \hat{\mathbf{X}}_i} [\|\mathbf{X}_i - \hat{\mathbf{X}}_i\|_2^2]. \quad (13)$$

- **Consistency Loss of Complex Spectra:** Due to the separate estimation of magnitude and phase spectra, when they are combined to reconstruct the enhanced waveform using ISTFT, the short-time spectral inconsistency between the estimated complex spectrum $(\hat{\mathbf{X}}_r, \hat{\mathbf{X}}_i)$ and the re-extracted complex spectrum $(\hat{\mathbf{X}}'_r, \hat{\mathbf{X}}'_i)$ from the enhanced waveform is inevitable. The discrepancy between $(\hat{\mathbf{X}}_r, \hat{\mathbf{X}}_i)$ and $(\hat{\mathbf{X}}'_r, \hat{\mathbf{X}}'_i)$ is the consistency gap, which needs to be narrowed. Here we define the consistency loss $\mathcal{L}_{\text{Con.}}$ between their real and imaginary parts as follows:

$$\mathcal{L}_{\text{Con.}} = \mathbb{E}_{\hat{\mathbf{X}}_r, \hat{\mathbf{X}}'_r} [\|\hat{\mathbf{X}}_r - \hat{\mathbf{X}}'_r\|_2^2] + \mathbb{E}_{\hat{\mathbf{X}}_i, \hat{\mathbf{X}}'_i} [\|\hat{\mathbf{X}}_i - \hat{\mathbf{X}}'_i\|_2^2]. \quad (14)$$

The total loss defined on complex spectra is the sum of the MSE loss and consistency loss:

$$\mathcal{L}_{\text{Com.}} = \mathcal{L}_{\text{MSECom.}} + \mathcal{L}_{\text{Con.}}. \quad (15)$$

4) *The final loss for model training:* The final generator loss \mathcal{L}_{G} is the linear combination of $\mathcal{L}_{\text{Mag.}}$, $\mathcal{L}_{\text{Pha.}}$, and $\mathcal{L}_{\text{Com.}}$:

$$\mathcal{L}_{\text{G}} = \lambda_1 \mathcal{L}_{\text{Mag.}} + \lambda_2 \mathcal{L}_{\text{Pha.}} + \lambda_3 \mathcal{L}_{\text{Com.}}. \quad (16)$$

where λ_1 , λ_2 , and λ_3 are hyperparameters. The training criteria of the MP-SENet is to jointly minimize \mathcal{L}_{G} and \mathcal{L}_{D} .

IV. EXPERIMENTAL SETUP

A. Datasets

1) *Denoising:* We used the publicly available Voice-Bank+DEMAND dataset [73] for speech denoising experiments, which includes pairs of clean and noisy audio clips with a sampling rate of 48 kHz. All the audio clips were resampled

to 16 kHz in the experiments. The clean audio set is selected from the Voice Bank corpus [74], which consists of 11,572 audio clips from 28 speakers for training and 824 audio clips from 2 unseen speakers for testing. The clean audio clips are mixed with 10 types of noise (8 types from the DEMAND database [75] and 2 artificial types) at SNRs of 0dB, 5dB, 10dB, and 15 dB for the training set and 5 types of unseen noise from the DEMAND database at SNRs of 2.5 dB, 7.5dB, 12.5 dB, and 17.5 dB for the test set.

2) *Dereverberation:* We used the same clean dataset with a sampling rate of 16kHz as in the denoising experiments and created reverberant speech data by convolving RIRs with the clean data for our dereverberation experiments. In addition, we selected 560 audio clips from the training set for validation. For the training and validation sets, the clean audio clips are convolved with RIRs at two microphone positions selected from five rooms: booth (210 ms), office (574 ms), and lecture (827 ms) in AIR database [76], medium size room (341 ms) in MIRD database [77], and reflective room (523 ms)¹ in MARDY database [78]. For the test set, RIRs at two microphone positions are selected from three rooms: small room (188 ms) and large room (593 ms) in MIRD database [77], and meeting room (300 ms) in AIR database [76].

3) *Bandwidth extension:* We used the VCTK dataset [79] which contains 44 hours of speech recordings from 108 speakers with a sampling rate of 48 kHz for our bandwidth extension experiments. For a fair comparison, we followed the task design of [57]. For the single-speaker experiment, we selected audio clips of a specific speaker (speaker p225). We used the first 223 audio clips for training and the remaining 8 for testing. For the multi-speaker experiment, we split the entire set of 44,257 audio clips into 88% training, 6% validation, and 6% testing, with no speaker overlap. We resampled all the audio clips to a sampling rate of 16 kHz and used them as the wideband reference samples. To obtain the narrowband audio clips, we first subsampled the 16 kHz ones with a rate of R and then upsampled them back to 16 kHz via interpolation. We set R to 2 and 4 in both the single-speaker and multi-speaker experiments, indicating the extensions from 8 kHz and 4 kHz to 16 kHz, respectively.

B. Model Configuration

In the training stage, all the audio clips were sliced into 2-second segments. To extract input features from raw waveforms using STFT, the FFT point number, Hanning window size, and hop size were set to 400, 400 (25 ms), and 100 (6.25 ms), respectively. Thus the number of frequency bins $F = 201$, while the number of feature frames depends on the audio lengths. For training our proposed MP-SENet, we set the batch size B , the number of channels C , the number of TF-Transformer blocks N , and the number of heads in the MHSA M to 4, 64, 4, and 4, respectively. The hyperparameters γ_1 and γ_2 in the magnitude loss $\mathcal{L}_{\text{Mag.}}$ were set to 1 and 0.05. The hyperparameters λ_1 , λ_2 , and λ_3 in the generator loss \mathcal{L}_{G} were set to 0.9, 0.3, and 0.1, respectively. All the

¹The numbers in (·) represent the average reverberation time T60 on two microphone positions calculated using the tools provided in [77].

models were trained using the AdamW optimizer [80], with $\beta_1 = 0.8$, $\beta_2 = 0.99$, and weight decay of 0.01. For speech denoising, dereverberation, and bandwidth extension single-speaker experiments, we trained all the models until 120 epochs. For bandwidth extension multi-speaker experiments, we trained our model to 500k steps. The learning rate was set initially to 0.0005 and scheduled to decay with a factor of 0.99 at every epoch.²

C. Evaluation Metrics

1) *Denoising*: For the speech denoising task, five commonly used objective evaluation metrics were chosen to evaluate the enhanced speech quality, including wideband PESQ, STOI, and three composite measures (i.e., CSIG, CBAK, and COVL). PESQ was used to evaluate the perceptual speech quality, which ranges from -0.5 to 4.5. STOI was used to measure speech intelligibility, which ranges from 0 to 1. CSIG, CBAK, and COVL measure signal distortion, background noise intrusiveness, and overall effect, respectively. All these three mean opinion score (MOS) based metrics range from 1 to 5. For all the metrics, higher values indicate better performance.

2) *Dereverberation*: For the speech dereverberation task, we adopted the same objective evaluation metrics as used in [15], which includes PESQ, cepstral distance (CD), log-likelihood ratio (LLR), frequency-weighted segmental signal-to-noise ratio (FWSegSNR), and signal-to-reverberation modulation energy ratio (SRMR). Except for SRMR, the calculation of other metrics requires corresponding reference speech. For CD and LLR, lower values indicate better performance; for other metrics, higher values indicate better performance.

3) *Bandwidth extension*: In the task of denoising and dereverberation, it is common practice to solely use objective metrics to evaluate the performance of models. However, for bandwidth extension, we employed both objective and subjective evaluations as other works to compare the performance of our proposed MP-SENet with other advanced bandwidth extension methods in terms of enhanced speech quality.

For objective evaluation, we included PESQ and log-spectral distance (LSD) as evaluation metrics. LSD was used to measure the logarithmic distance between two magnitude spectra in dB. Higher PESQ scores and lower LSD values indicate better performance.

Regarding subjective evaluation, we conducted ABX preference tests on the Amazon Mechanical Turk platform³ to compare the performance between two comparative systems. For the VCTK single-speaker experiment, all eight utterances in the test set were utilized. For the VCTK multi-speaker experiment, we randomly selected 20 utterances from the test set for evaluation. Each ABX test was assessed by a minimum of 30 native English listeners. These listeners were required to judge which utterance in each pair exhibited better speech quality or if there was no preference. To calculate the average preference scores, the p -value of a t -test was conducted to

measure the significance of the difference between each pair of systems.

V. RESULTS AND ANALYSIS

A. Comparison with Advanced SE Methods

1) *Denoising*: For speech denoising, we compared our proposed MP-SENet with several representative time-domain and TF-domain methods. In the time-domain category, we included SEGAN [6], DEMUCS [8], and SE-Conformer [9]. For the TF-domain methods, we selected MetricGAN [23], PHASEN [30], MetricGAN+ [69], and four SOTA methods, namely DPT-FSNet [13], TridentSE [14], DB-AIAT [17], and CMGAN [19].

The objective evaluation results are presented in Table I. Clearly, our proposed MP-SENet outperformed all other speech denoising methods across all metrics, demonstrating its strong denoising capability. From Table I, it is evident that time-domain methods generally perform inferior to TF-domain methods. Inside the TF-domain methods, only our proposed MP-SENet and PHASEN used both magnitude and phase spectra as input conditions. In spite of that, when compared to PHASEN, our proposed MP-SENet exhibited significant improvements of 0.61, 0.60, 0.44, and 0.72 in PESQ, CSIG, CBAK, and COVL scores with a nine times smaller model size. These improvements validated the effectiveness of explicit phase optimization in our proposed MP-SENet. Furthermore, when compared to the four TF-domain SOTA approaches, MP-SENet still performed the best on all the objective metrics. Overall, our proposed MP-SENet achieved a new SOTA performance with a PESQ of 3.60 and a moderate model size of 2.26M parameters.

For more evidence, we visualized the spectrograms of speech signals enhanced by MP-SENet and CMGAN as shown in Fig. 5a. By comparing the contents of boxes with the same color, we can see that the MP-SENet mitigated the damage to harmonic structures that occurred in CMGAN. This result indicated that predicting the phase directly instead of relying on complex spectrum refinement can further alleviate the bidirectional compensation effect between magnitude and phase and preserve the harmonic structures.

Paliwal *et al.* [5] emphasized the importance of phase information for speech denoising tasks in low-SNR circumstances. Theoretically, The noisy phase \mathbf{Y}_p can be derived as follows [81]:

$$\begin{aligned} \mathbf{Y}_p &= \arg(\mathbf{X}_m e^{j\mathbf{X}_p} + \mathbf{N}_m e^{j\mathbf{N}_p}) \\ &= \mathbf{X}_p + \arg\left(1 + \frac{\mathbf{N}_m}{\mathbf{X}_m} e^{j(\mathbf{N}_p - \mathbf{X}_p)}\right), \end{aligned} \quad (17)$$

where $\mathbf{N}_m \in \mathbb{R}^{T \times F}$ and $\mathbf{N}_p \in \mathbb{R}^{T \times F}$ denote the magnitude and phase spectra of the noise signal $\mathbf{n} \in \mathbb{R}^L$, respectively. $\arg(\cdot)$ calculates the phase spectrum of a complex spectrum. When in a high-SNR circumstance, the clean magnitude spectrum \mathbf{X}_m is much larger than the noise magnitude spectrum \mathbf{N}_m , the second term in Eq. 17 would approach zero, indicating that the clean phase spectrum \mathbf{X}_p can be approximated by the noisy phase spectrum \mathbf{Y}_p . So we hypothesized that as the SNR increases, the contribution of phase information to the performance of the SE model would diminish.

²Source codes will be released after paper acceptance, audio samples can be found at <https://yxl-0102.github.io/MP-SENet-demo>.

³<https://www.mturk.com>.

TABLE I
EXPERIMENTAL RESULTS FOR SPEECH DENOISING METHODS EVALUATED ON THE VOICEBANK+DEMAND DATASET. “-” DENOTES THE RESULT THAT IS NOT PROVIDED IN THE ORIGINAL PAPER.

Method	Year	Input	#Param.	PESQ	CSIG	CBAK	COVL	STOI
Noisy	-	-	-	1.97	3.35	2.44	2.63	0.91
SEGAN [6]	2017	Waveform	43.2M	2.16	3.48	2.94	2.80	0.92
DEMUCS [8]	2021	Waveform	33.5M	3.07	4.31	3.40	3.63	0.95
SE-Conformer [9]	2021	Waveform	-	3.13	4.45	3.55	3.82	0.95
MetricGAN [23]	2019	Magnitude	-	2.86	3.99	3.18	3.42	-
MetricGAN+ [69]	2021	Magnitude	-	3.15	4.14	3.16	3.64	-
DPT-FSNet [13]	2021	Complex	0.88M	3.33	4.58	3.72	4.00	0.96
TridentSE [14]	2023	Complex	3.03M	3.47	4.70	3.81	4.10	0.96
DB-AIAT [17]	2021	Magnitude+Complex	2.81M	3.31	4.61	3.75	3.96	-
CMGAN [19]	2022	Magnitude+Complex	1.83M	3.41	4.63	3.94	4.12	0.96
PHASEN [30]	2020	Magnitude+Phase	20.9M	2.99	4.21	3.55	3.62	-
MP-SENet	2023	Magnitude+Phase	2.26M	3.60	4.81	3.99	4.34	0.96

TABLE II
EXPERIMENTAL RESULTS UNDER DIFFERENT SNR CONDITIONS.

SNR	Method	PESQ	CSIG	CBAK	COVL	STOI
2.5dB	Noisy	1.51	2.90	1.99	2.19	0.88
	CMGAN	3.04	4.38	3.62	3.77	0.94
	MP-SENet	3.25	4.61	3.69	4.01	0.95
7.5dB	Noisy	1.82	3.35	2.40	2.59	0.92
	CMGAN	3.39	4.66	3.88	4.11	0.96
	MP-SENet	3.57	4.84	3.93	4.32	0.96
12.5dB	Noisy	2.22	3.81	2.87	3.05	0.94
	CMGAN	3.67	4.85	4.12	4.39	0.97
	MP-SENet	3.80	4.95	4.14	4.54	0.97
17.5dB	Noisy	2.69	4.26	3.41	3.54	0.96
	CMGAN	3.89	4.95	4.35	4.61	0.98
	MP-SENet	3.98	4.99	4.35	4.71	0.98

To experimentally verify our hypothesis, we conducted an analysis experiment in which we tested the performance of our proposed MP-SENet under different SNR circumstances. Additionally, we selected CMGAN, which implicitly enhances the phase, as a comparative system to validate the importance of explicit phase enhancement. With the clean test set of the Voice Bank corpus, we re-noised it with five types of unseen noise (i.e., living room, office space, bus, open area cafeteria, and a public square) in the training set under 5 separate SNR conditions (i.e., 2.5 dB, 7.5dB, 12.5 dB, and 17.5 dB). Subsequently, we employed these 5 test sets with varying SNR levels to evaluate the performance of CMGAN and our proposed MP-SENet. The experimental results are presented in Table. II, and it is evident that as the SNR increased from 2.5 dB to 17.5 dB, our proposed MP-SENet with precise phase enhancement demonstrated improvements of 6.9%, 5.3%, 3.5%, and 2.3% in PESQ compared to CMGAN. For other metrics, the degree of their improvements compared to those of CMGAN also became smaller as the SNR increased. These findings aligned with our hypothesis and highlighted the significance of recovering phase information in

TABLE III
EXPERIMENTAL RESULTS FOR SPEECH DEREVERBERATION METHODS.

Method	PESQ	CD	LLR	FWSegSNR	SRMR
Reverbrant	1.84	3.67	0.66	6.09	6.62
NARA-WPE [46]	2.03	3.51	0.66	6.33	7.27
SkipConvNet [15]	2.35	2.82	0.28	10.31	8.84
CMGAN [20]	2.68	2.97	0.27	10.38	9.48
MP-SENet	2.97	2.64	0.24	11.53	10.77

low-SNR circumstances. Therefore, our proposed MP-SENet could exhibit superior performance when applied under low-SNR conditions, such as communication systems in aircraft, railways, or noisy public areas.

2) *Dereverberation*: For speech dereverberation, we compared our proposed MP-SENet with NARA-WPE [46], a signal processing-based method, as well as two advanced DNN-based methods, namely SkipConvNet [15] and CMGAN [20]. For NARA-WPE, we employed a configuration with a three-sample delay and a ten-tap filter size. We performed a total of 15 iterations on each audio clip to estimate the filter weights used for dereverberating the speech signal. SkipConvNet adopts an encoder-decoder architecture with multiple convolutional modules to learn a non-linear mapping from a reverberant speech log-power spectrum to an anechoic one. We enhanced our reverberant dataset with the open-source implementations of SkipConvNet⁴ and CMGAN⁵.

The objective evaluation results are presented in Table. III. It’s obvious that our proposed MP-SENet surpassed all other speech dereverberation methods among all the metrics. Specifically, DNN-based methods exhibited more robust dereverberation capabilities compared to signal processing-based methods. Among the DNN-based methods, compared to SkipConvNet, CMGAN achieved an apparent improvement in PESQ by employing a metric discriminator, while their differences in other metrics were relatively small. Our proposed MP-

⁴<https://github.com/zehuachenImperial/SkipConvNet>.

⁵<https://github.com/ruizhecao96/CMGAN>.

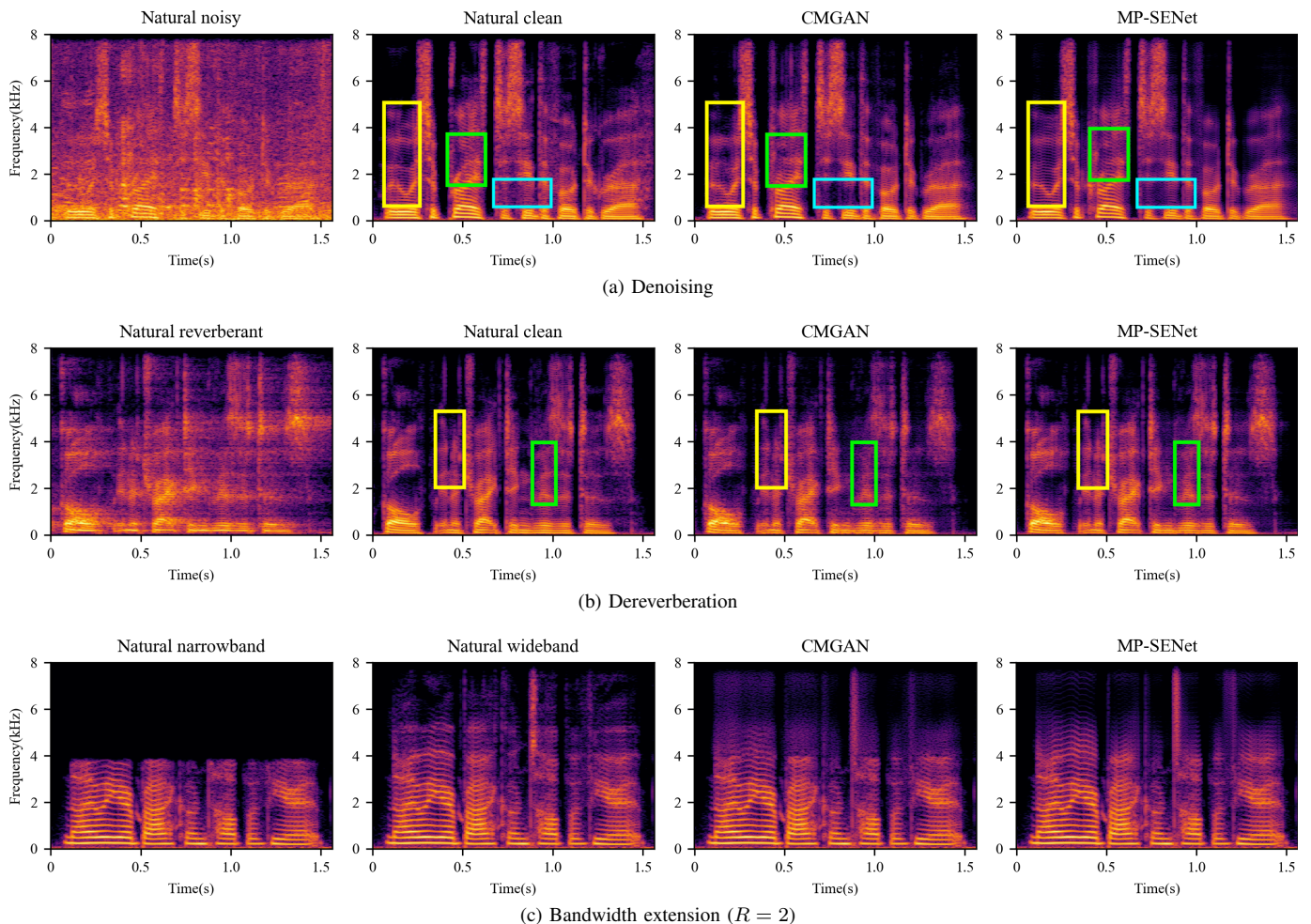


Fig. 5. Spectrogram visualization of the distorted speech signal, original speech signal, and speech signals enhanced by CMGAN and our proposed MP-SENet.

SENet also adopted a metric discriminator to achieve a promising PESQ score. Nevertheless, MP-SENet introduced explicit phase estimation and optimization, resulting in significant improvements across all the metrics compared to CMGAN, demonstrating the importance of phase information to speech dereverberation.

We also visualized the spectrograms of speech signals enhanced by MP-SENet and CMGAN as shown in Fig. 5b. In general, the spectrogram of the enhanced speech by MP-SENet appeared slightly brighter compared to CMGAN, which indicated a higher energy level and aligned with their SRMR scores. By comparing the contents of boxes with the same color, we observed that the harmonic components of the speech enhanced by CMGAN still exhibited smearing artifacts, while MP-SENet effectively mitigated this issue.

3) *Bandwidth extension*: For bandwidth extension, we conducted both objective and subjective evaluations to assess the performance of our proposed MP-SENet. For objective evaluation, we compared MP-SENet with two time-domain methods (i.e., AudioUNet [11] and Wang *et al.* [57]), a TF-domain method (i.e., CMGAN [20]), and a hybrid-domain method (i.e., TFNet [56]). Except for CMGAN which we used its open-source implementation to reproduce the results, all other objective results were selected from [57]. Regarding subjective

evaluation, we solely selected the suboptimal CMGAN as the comparative system according to the objective results.

The objective evaluation results are presented in Table IV. For a subsampling factor of $R = 2$, which indicates the recovery of 16 kHz speech waveforms from 8 kHz ones, our proposed MP-SENet achieved the highest scores in terms of PESQ and LSD for both single-speaker and multi-speaker experiments. For a subsampling factor of $R = 4$, our proposed MP-SENet still performed the best in the VCTK single-speaker experiment, but worse than the method proposed by Wang *et al.* in terms of PESQ in VCTK multi-speaker experiments. Sometimes, objective metrics may not fully reflect the model performance, so we further conducted subjective experiments to complement the validation of objective metrics.

The subjective ABX test results are illustrated in Fig. 6. In the single-speaker experiments, whether the waveforms recovered from the sampling rate of 8kHz or 4kHz, our proposed MP-SENet significantly outperformed CMGAN in generating 16kHz waveforms ($p < 0.01$). In the multi-speaker experiments, our proposed MP-SENet performed slightly better than CMGAN for both $R = 2$ and $R = 4$ (p is slightly higher than 0.01). This difference highlighted the strong bandwidth extension capability of our proposed MP-SENet, even in data-constrained circumstances. Furthermore, it suggested that the

TABLE IV
EXPERIMENTAL RESULTS FOR BANDWIDTH EXTENSION METHODS ON THE VCTK DATASET.

Method	R	VCTK-single		VCTK-multi.	
		PESQ	LSD	PESQ	LSD
AudioUNet [11]	2	3.90	1.36	3.68	1.32
TFNet [56]		3.91	1.24	3.72	0.99
Wang <i>et al.</i> [57]		4.17	0.94	3.91	0.88
CMGAN [20]		4.18	0.74	4.10	0.73
MP-SENet		4.32	0.70	4.23	0.71
AudioUNet [11]	4	3.40	1.41	3.39	1.40
TFNet [56]		3.49	1.33	3.48	1.22
Wang <i>et al.</i> [57]		3.51	0.94	3.64	0.95
CMGAN [20]		3.68	0.91	3.41	1.17
MP-SENet		3.86	0.85	3.57	0.91

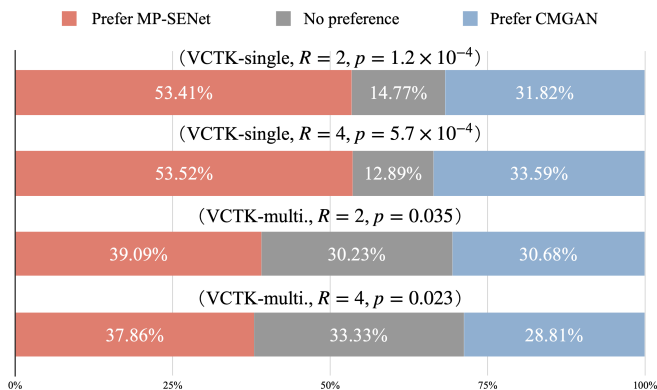


Fig. 6. Average preference scores (%) of ABX tests on speech quality between MP-SENet and CMGAN in the bandwidth extension task, p denotes the p -value of a t -test between two systems.

advantage of our model weakened in multi-speaker scenarios, which aligned with the objective evaluation results.

We still visualized the spectrograms of speech signals enhanced by MP-SENet and CMGAN with $R = 2$ as shown in Fig. 5c. By comparing the high-frequency components of the spectrograms, we can observe that the MP-SENet demonstrated a strong capability in restoring high-frequency harmonics, which confirms the importance of phase information in bandwidth extension tasks.

B. Ablation Studies

To investigate the role of each key component in the MP-SENet, we took the denoising task as the ablation example and performed ablation studies on the VoiceBank+DEMAND dataset. We initially performed ablation studies to validate the contributions of specific modules within our model. Then, we performed ablation of certain losses to assess the impact of different optimization approaches on model performance. The ablation results are presented in Table. V.

1) *Ablation studies on modules*: We first conducted ablation studies on the TF-Transformer blocks. To compare their capability of capturing long-term correlations with the Conformer-based ones used in CMGAN, we replaced the Transformers with Conformers (*w/o* Trans.). The ablation of the Transformers resulted in performance degradation, which may be

TABLE V
EXPERIMENTAL RESULTS OF THE ABLATION STUDIES ON THE VOICEBANK+DEMAND DATASET.

Method	#Param.	PESQ	CSIG	CBAK	COVL
MP-SENet	2.26M	3.60	4.81	3.99	4.34
<i>w/o</i> Trans.	1.77M	3.56	4.77	3.96	4.30
Parallel Trans.	2.26M	3.58	4.78	3.96	4.30
Freq.→Time	2.26M	3.60	4.79	3.98	4.33
<i>w/o</i> Mag. dec.	1.99M	3.58	4.79	3.92	4.32
<i>w/o</i> Pha. dec.	1.99M	3.44	4.71	3.83	4.18
<i>w/o</i> Pha. loss	2.26M	3.55	4.77	3.96	4.28
<i>w/o</i> Com. loss	2.26M	3.57	4.80	3.93	4.32
<i>w/o</i> Con. loss	2.26M	3.58	4.81	3.97	4.32
<i>w/o</i> Metric disc.	2.26M	3.44	4.72	3.94	4.20
CMGAN [19]	1.83M	3.41	4.63	3.94	4.12

attributed to the fact that Transformers are better at capturing contextual dependencies compared to Conformers. However, it was noteworthy that our MP-SENet with Conformers still outperformed CMGAN in most metrics with a smaller model size (1.77M) compared to that of CMGAN (1.83M). This result indicated that, with the same attention-based module to capture both local and global information, our proposed explicit phase enhancement method exhibits substantial superiority compared to the implicit one. Subsequently, we changed the stack style of the Time- and Freq.-Transformers from a sequential manner to a parallel manner (Parallel Trans.) as used in DB-AIAT [17]. As a result, all the metrics slightly decreased, which indicated the sequential stacking mode was superior. With the sequential manner of the time and frequency Transformers, we reversed their order from Time→Freq. to Freq.→Time and observed a minimal decrease in three MOS-based metrics, suggesting that the order had a negligible impact on the model performance.

Furthermore, we investigated the effect of magnitude and phase modeling. We first removed the magnitude decoder (“*w/o* Mag. dec.”) to ask the phase decoder to directly output the real and imaginary parts of the complex spectrum. Consequently, all the metrics marginally degraded, which demonstrated that implicit magnitude and phase modeling can still achieve exceptional enhancement performance under the guidance of explicit magnitude and phase optimization. Subsequently, we removed the phase decoder and combined the enhanced magnitude spectrum with the distorted phase spectrum to generate a waveform (“*w/o* Pha. dec.”). As a consequence, all the metrics significantly degraded. Therefore, we concluded that explicit phase estimation is indispensable and considerably contributes to the enhancement performance.

2) *Ablation studies on loss functions*: We further conducted ablation studies on the loss functions. To investigate the effects of phase optimization approaches, we conducted ablation studies on the phase loss (“*w/o* Pha. loss”) and complex loss (“*w/o* Com. loss”), which explicitly and implicitly optimized the phase, respectively. Results demonstrated that both of them contributed to the overall performance, but explicit phase optimization played a more pivotal role in SE tasks. Subsequently, we solely ablated the consistency loss of complex spectra (*w/o*

Con. loss) and the results demonstrated that the short-time spectral consistency did contribute to the model performance. Finally, we removed the metric discriminator (“*w/o* Metric disc.”) to assess the effect of the human-perception-related metric loss. Ablation results demonstrated that metric loss remarkably improves model performance in terms of speech perceptual quality. Surprisingly, our proposed MP-SENet without discriminator was still capable of high-quality SE, and its performance even surpassed that of CMGAN.

VI. CONCLUSION

In this paper, we proposed an SE model called MP-SENet, which directly enhanced both magnitude and phase spectra in parallel. The overall structure of the MP-SENet was a codec architecture, where the encoder encoded distorted magnitude and phase spectra to TF-domain representations, and the parallel magnitude decoder and phase decoder output the enhanced magnitude and phase spectra, respectively. The encoder and decoder are bridged by TF-Transformers to capture time and frequency dependencies. The major breakthrough of the MP-SENet lay in the explicit modeling and optimization of the phase spectrum. Experimental results demonstrated that our proposed MP-SENet was capable of high-quality SE across speech denoising, speech dereverberation, and bandwidth extension tasks. Especially for the speech denoising task, our proposed MP-SENet has achieved a SOTA performance on the public VoiceBank+DEMAND dataset with a PESQ of 3.60. Spectrogram visualizations demonstrated the powerful harmonic restoration capability of our MP-SENet, indicating that explicit magnitude and phase enhancement can effectively alleviate the compensation effect between them and significantly improve the enhancement performance. Moreover, ablation studies verified the effectiveness of each component and optimization method in the MP-SENet. Further reducing the model parameters and improving the inference efficiency will be the focus of our future work.

REFERENCES

- [1] Y.-X. Lu, Y. Ai, and Z.-H. Ling, “MP-SENet: A speech enhancement model with parallel denoising of magnitude and phase spectra,” in *Proc. Interspeech*, 2023.
- [2] F. Weninger, H. Erdogan, S. Watanabe, E. Vincent, J. Le Roux, J. R. Hershey, and B. Schuller, “Speech enhancement with LSTM recurrent neural networks and its application to noise-robust ASR,” in *International Conference on Latent Variable Analysis and Signal Separation (LVA/ICA)*, 2015, pp. 91–99.
- [3] J. L. Desjardins and K. A. Doherty, “The effect of hearing aid noise reduction on listening effort in hearing-impaired adults,” *Ear and hearing*, vol. 35, no. 6, pp. 600–610, 2014.
- [4] D. Wang and J. Lim, “The unimportance of phase in speech enhancement,” *IEEE/ACM Transactions on Acoustics, Speech, and Signal Processing*, vol. 30, no. 4, pp. 679–681, 1982.
- [5] K. Paliwal, K. Wójcicki, and B. Shannon, “The importance of phase in speech enhancement,” *Speech Communication*, vol. 53, no. 4, pp. 465–494, 2011.
- [6] S. Pascual, A. Bonafonte, and J. Serrà, “SEGAN: Speech enhancement generative adversarial network,” in *Proc. Interspeech*, 2017, pp. 3642–3646.
- [7] A. Pandey and D. Wang, “TCNN: Temporal convolutional neural network for real-time speech enhancement in the time domain,” in *Proc. ICASSP*, 2019, pp. 6875–6879.
- [8] A. Défossez, G. Synnaeve, and Y. Adi, “Real time speech enhancement in the waveform domain,” in *Proc. Interspeech*, 2020, pp. 3291–3295.
- [9] E. Kim and H. Seo, “SE-Conformer: Time-domain speech enhancement using conformer,” in *Proc. Interspeech*, 2021, pp. 2736–2740.
- [10] Z. Kong, W. Ping, A. Dantrey, and B. Catanzaro, “Speech denoising in the waveform domain with self-attention,” in *Proc. ICASSP*, 2022, pp. 7867–7871.
- [11] V. Kuleshov, S. Z. Enam, and S. Ermon, “Audio super-resolution using neural nets,” in *Proc. ICLR (Workshop Track)*, 2017.
- [12] K. Tan and D. Wang, “Learning complex spectral mapping with gated convolutional recurrent networks for monaural speech enhancement,” *IEEE/ACM Transactions on Audio, Speech, and Language Processing*, vol. 28, pp. 380–390, 2019.
- [13] F. Dang, H. Chen, and P. Zhang, “DPT-FSNet: Dual-path transformer based full-band and sub-band fusion network for speech enhancement,” in *Proc. ICASSP*, 2022, pp. 6857–6861.
- [14] D. Yin, Z. Zhao, C. Tang, Z. Xiong, and C. Luo, “TridentSE: Guiding speech enhancement with 32 global tokens,” in *Proc. Interspeech*, 2023.
- [15] V. Kothapally, W. Xia, S. Ghorbani, J. H. Hansen, W. Xue, and J. Huang, “SkipConvNet: Skip convolutional neural network for speech dereverberation using optimally smoothed spectral mapping,” in *Proc. Interspeech*, 2020, pp. 3935–3939.
- [16] Z.-Q. Wang, G. Wichern, and J. Le Roux, “On the compensation between magnitude and phase in speech separation,” *IEEE Signal Processing Letters*, vol. 28, pp. 2018–2022, 2021.
- [17] G. Yu, A. Li, C. Zheng, Y. Guo, Y. Wang, and H. Wang, “Dual-branch attention-in-attention transformer for single-channel speech enhancement,” in *Proc. ICASSP*, 2022, pp. 7847–7851.
- [18] G. Yu, A. Li, H. Wang, Y. Wang, Y. Ke, and C. Zheng, “DBT-Net: Dual-branch federative magnitude and phase estimation with attention-in-attention transformer for monaural speech enhancement,” *IEEE/ACM Transactions on Audio, Speech, and Language Processing*, vol. 30, pp. 2629–2644, 2022.
- [19] R. Cao, S. Abdulatif, and B. Yang, “CMGAN: Conformer-based Metric GAN for Speech Enhancement,” in *Proc. Interspeech*, 2022, pp. 936–940.
- [20] S. Abdulatif, R. Cao, and B. Yang, “CMGAN: Conformer-based metric-gan for monaural speech enhancement,” *arXiv preprint arXiv:2209.11112*, 2022.
- [21] A. Vaswani, N. Shazeer, N. Parmar, J. Uszkoreit, L. Jones, A. N. Gomez, Ł. Kaiser, and I. Polosukhin, “Attention is all you need,” *Advances in neural information processing systems*, vol. 30, 2017.
- [22] Y. Ai and Z.-H. Ling, “Neural speech phase prediction based on parallel estimation architecture and anti-wrapping losses,” in *Proc. ICASSP*, 2023.
- [23] S.-W. Fu, C.-F. Liao, Y. Tsao, and S.-D. Lin, “MetricGAN: Generative adversarial networks based black-box metric scores optimization for speech enhancement,” in *Proc. ICML*, 2019, pp. 2031–2041.
- [24] Y. Xu, J. Du, L.-R. Dai, and C.-H. Lee, “A regression approach to speech enhancement based on deep neural networks,” *IEEE/ACM Transactions on Audio, Speech, and Language Processing*, vol. 23, no. 1, pp. 7–19, 2014.
- [25] C. Valentini-Botinhao and J. Yamagishi, “Speech enhancement of noisy and reverberant speech for text-to-speech,” *IEEE/ACM Transactions on Audio, Speech, and Language Processing*, vol. 26, no. 8, pp. 1420–1433, 2018.
- [26] Y. Ai, J.-X. Zhang, L. Chen, and Z.-H. Ling, “DNN-based spectral enhancement for neural waveform generators with low-bit quantization,” in *Proc. ICASSP*, 2019, pp. 7025–7029.
- [27] J. Kim, M. El-Khamy, and J. Lee, “T-GSA: Transformer with Gaussian-weighted self-attention for speech enhancement,” in *Proc. ICASSP*, 2020, pp. 6649–6653.
- [28] V. Kothapally and J. H. Hansen, “Skipconvgan: Monaural speech dereverberation using generative adversarial networks via complex time-frequency masking,” *IEEE/ACM Transactions on Audio, Speech, and Language Processing*, vol. 30, pp. 1600–1613, 2022.
- [29] A. Gulati, J. Qin, C.-C. Chiu, N. Parmar, Y. Zhang, J. Yu, W. Han, S. Wang, Z. Zhang, Y. Wu *et al.*, “Conformer: Convolution-augmented transformer for speech recognition,” in *Proc. Interspeech*, 2020, pp. 5036–5040.
- [30] D. Yin, C. Luo, Z. Xiong, and W. Zeng, “PHASEN: A phase-and-harmonics-aware speech enhancement network,” in *Proc. AAAI*, vol. 34, no. 05, 2020, pp. 9458–9465.
- [31] M. Krawczyk and T. Gerkmann, “STFT phase reconstruction in voiced speech for an improved single-channel speech enhancement,” *IEEE/ACM Transactions on Audio, Speech, and Language Processing*, vol. 22, no. 12, pp. 1931–1940, 2014.

- [32] P. Mowlaee and J. Kulmer, "Harmonic phase estimation in single-channel speech enhancement using phase decomposition and snr information," *IEEE/ACM Transactions on Audio, Speech, and Language Processing*, vol. 23, no. 9, pp. 1521–1532, 2015.
- [33] M. Berouti, R. Schwartz, and J. Makhoul, "Enhancement of speech corrupted by acoustic noise," in *Proc. ICASSP*, vol. 4, 1979, pp. 208–211.
- [34] J. Lim and A. Oppenheim, "All-pole modeling of degraded speech," *IEEE Transactions on Acoustics, Speech, and Signal Processing*, vol. 26, no. 3, pp. 197–210, 1978.
- [35] Y. Ephraim, "Statistical-model-based speech enhancement systems," *Proceedings of the IEEE*, vol. 80, no. 10, pp. 1526–1555, 1992.
- [36] M. Dendrinos, S. Bakamidis, and G. Carayannis, "Speech enhancement from noise: A regenerative approach," *Speech Communication*, vol. 10, no. 1, pp. 45–57, 1991.
- [37] Y. Ephraim and H. L. Van Trees, "A signal subspace approach for speech enhancement," *IEEE Transactions on speech and audio processing*, vol. 3, no. 4, pp. 251–266, 1995.
- [38] Y. Xu, J. Du, L.-R. Dai, and C.-H. Lee, "An experimental study on speech enhancement based on deep neural networks," *IEEE Signal processing letters*, vol. 21, no. 1, pp. 65–68, 2013.
- [39] G. Hu and D. Wang, "Speech segregation based on pitch tracking and amplitude modulation," in *Proc. WASPAA*, 2001, pp. 79–82.
- [40] S. Srinivasan, N. Roman, and D. Wang, "Binary and ratio time-frequency masks for robust speech recognition," *Speech Communication*, vol. 48, no. 11, pp. 1486–1501, 2006.
- [41] A. Narayanan and D. Wang, "Ideal ratio mask estimation using deep neural networks for robust speech recognition," in *Proc. ICASSP*, 2013, pp. 7092–7096.
- [42] Y. Wang, A. Narayanan, and D. Wang, "On training targets for supervised speech separation," *IEEE/ACM Transactions on Audio, Speech, and Language Processing*, vol. 22, no. 12, pp. 1849–1858, 2014.
- [43] H. Erdogan, J. R. Hershey, S. Watanabe, and J. Le Roux, "Phase-sensitive and recognition-boosted speech separation using deep recurrent neural networks," in *Proc. ICASSP*, 2015, pp. 708–712.
- [44] D. S. Williamson, Y. Wang, and D. Wang, "Complex ratio masking for monaural speech separation," *IEEE/ACM Transactions on Audio, Speech, and Language Processing*, vol. 24, no. 3, pp. 483–492, 2015.
- [45] T. Nakatani, T. Yoshioka, K. Kinoshita, M. Miyoshi, and B.-H. Juang, "Speech dereverberation based on variance-normalized delayed linear prediction," *IEEE/ACM Transactions on Audio, Speech, and Language Processing*, vol. 18, no. 7, pp. 1717–1731, 2010.
- [46] L. Drude, J. Heymann, C. Boeddeker, and R. Haeb-Umbach, "NARA-WPE: A python package for weighted prediction error dereverberation in Numpy and Tensorflow for online and offline processing," in *Speech Communication; 13th ITG-Symposium*. VDE, 2018, pp. 1–5.
- [47] N. Roman and J. Woodruff, "Intelligibility of reverberant noisy speech with ideal binary masking," *The Journal of the Acoustical Society of America*, vol. 130, no. 4, pp. 2153–2161, 2011.
- [48] Y. Zhao, D. Wang, I. Merks, and T. Zhang, "DNN-based enhancement of noisy and reverberant speech," in *Proc. ICASSP*, 2016, pp. 6525–6529.
- [49] X. Li, J. Li, and Y. Yan, "Ideal ratio mask estimation using deep neural networks for monaural speech segregation in noisy reverberant conditions," in *Proc. Interspeech*, 2017, pp. 1203–1207.
- [50] D. S. Williamson and D. Wang, "Speech dereverberation and denoising using complex ratio masks," in *Proc. ICASSP*, 2017, pp. 5590–5594.
- [51] K. Han, Y. Wang, D. Wang, W. S. Woods, I. Merks, and T. Zhang, "Learning spectral mapping for speech dereverberation and denoising," *IEEE/ACM Transactions on Audio, Speech, and Language Processing*, vol. 23, no. 6, pp. 982–992, 2015.
- [52] O. Ernst, S. E. Chazan, S. Gannot, and J. Goldberger, "Speech dereverberation using fully convolutional networks," in *Proc. EUSIPCO*, 2018, pp. 390–394.
- [53] Z.-H. Ling, S.-Y. Kang, H. Zen, A. Senior, M. Schuster, X.-J. Qian, H. M. Meng, and L. Deng, "Deep learning for acoustic modeling in parametric speech generation: A systematic review of existing techniques and future trends," *IEEE Signal Processing Magazine*, vol. 32, no. 3, pp. 35–52, 2015.
- [54] J. Abel, M. Strake, and T. Fingscheidt, "A simple cepstral domain dnn approach to artificial speech bandwidth extension," in *Proc. ICASSP*, 2018, pp. 5469–5473.
- [55] K. Li and C.-H. Lee, "A deep neural network approach to speech bandwidth expansion," in *Proc. ICASSP*, 2015, pp. 4395–4399.
- [56] T. Y. Lim, R. A. Yeh, Y. Xu, M. N. Do, and M. Hasegawa-Johnson, "Time-frequency networks for audio super-resolution," in *Proc. ICASSP*, 2018, pp. 646–650.
- [57] H. Wang and D. Wang, "Towards robust speech super-resolution," *IEEE/ACM transactions on audio, speech, and language processing*, vol. 29, pp. 2058–2066, 2021.
- [58] A. Pandey and D. Wang, "Densely connected neural network with dilated convolutions for real-time speech enhancement in the time domain," in *Proc. ICASSP*, 2020, pp. 6629–6633.
- [59] D. Ulyanov, A. Vedaldi, and V. Lempitsky, "Instance normalization: The missing ingredient for fast stylization," *arXiv preprint arXiv:1607.08022*, 2016.
- [60] K. He, X. Zhang, S. Ren, and J. Sun, "Delving deep into rectifiers: Surpassing human-level performance on imagenet classification," in *Proc. ICCV*, 2015, pp. 1026–1034.
- [61] J. Chen, Q. Mao, and D. Liu, "Dual-path transformer network: Direct context-aware modeling for end-to-end monaural speech separation," in *Proc. Interspeech*, 2020, pp. 2642–2646.
- [62] K. Wang, B. He, and W.-P. Zhu, "TSTNN: Two-stage transformer based neural network for speech enhancement in the time domain," in *Proc. ICASSP*, 2021, pp. 7098–7102.
- [63] Y. Fu, Y. Liu, J. Li, D. Luo, S. Lv, Y. Jv, and L. Xie, "Uformer: A unet based dilated complex & real dual-path conformer network for simultaneous speech enhancement and dereverberation," in *Proc. ICASSP*, 2022, pp. 7417–7421.
- [64] Y. Li, Y. Sun, W. Wang, and S. M. Naqvi, "U-shaped transformer with frequency-band aware attention for speech enhancement," *IEEE/ACM Transactions on Audio, Speech, and Language Processing*, 2023.
- [65] J. L. Ba, J. R. Kiros, and G. E. Hinton, "Layer normalization," *arXiv preprint arXiv:1607.06450*, 2016.
- [66] X. Glorot, A. Bordes, and Y. Bengio, "Deep sparse rectifier neural networks," in *Proc. AISTATS*, 2011, pp. 315–323.
- [67] M. Sperber, J. Niehues, G. Neubig, S. Stüker, and A. Waibel, "Self-attentional acoustic models," *Proc. Interspeech*, pp. 3723–3727, 2018.
- [68] W. Shi, J. Caballero, F. Huszár, J. Totz, A. P. Aitken, R. Bishop, D. Rueckert, and Z. Wang, "Real-time single image and video super-resolution using an efficient sub-pixel convolutional neural network," in *Proc. CVPR*, 2016, pp. 1874–1883.
- [69] S.-W. Fu, C. Yu, T.-A. Hsieh, P. Plantinga, M. Ravanelli, X. Lu, and Y. Tsao, "MetricGAN+: An improved version of MetricGAN for speech enhancement," in *Proc. Interspeech*, 2021, pp. 201–205.
- [70] J. Benesty, S. Makino, and J. Chen, *Speech enhancement*. Springer Science & Business Media, 2006.
- [71] A. W. Rix, J. G. Beerends, M. P. Hollier, and A. P. Hekstra, "Perceptual evaluation of speech quality (pesq)—a new method for speech quality assessment of telephone networks and codecs," in *Proc. ICASSP*, vol. 2, 2001, pp. 749–752.
- [72] C. H. Taal, R. C. Hendriks, R. Heusdens, and J. Jensen, "An algorithm for intelligibility prediction of time-frequency weighted noisy speech," *IEEE/ACM Transactions on Audio, Speech, and Language Processing*, vol. 19, no. 7, pp. 2125–2136, 2011.
- [73] C. Valentini-Botinhao, X. Wang, S. Takaki, and J. Yamagishi, "Investigating RNN-based speech enhancement methods for noise-robust text-to-speech," in *Proc. SSW*, 2016, pp. 146–152.
- [74] C. Veaux, J. Yamagishi, and S. King, "The voice bank corpus: Design, collection and data analysis of a large regional accent speech database," in *Proc. O-COCOSDA/CASLRE*, 2013, pp. 1–4.
- [75] J. Thiemann, N. Ito, and E. Vincent, "The diverse environments multi-channel acoustic noise database (DEMAND): A database of multichannel environmental noise recordings," in *Proc. ICA*, vol. 19, no. 1, 2013, p. 035081.
- [76] M. Jeub, M. Schafer, and P. Vary, "A binaural room impulse response database for the evaluation of dereverberation algorithms," in *Proc. ICSDSP*, 2009, pp. 1–5.
- [77] E. Hadad, F. Heese, P. Vary, and S. Gannot, "Multichannel audio database in various acoustic environments," in *Proc. IWAENC*, 2014, pp. 313–317.
- [78] J. Y. Wen, N. D. Gaubitch, E. A. Habets, T. Myatt, and P. A. Naylor, "Evaluation of speech dereverberation algorithms using the mardy database," in *Proc. IWAENC*, 2006, pp. 1–4.
- [79] C. Veaux, J. Yamagishi, K. MacDonald *et al.*, "CSTR VCTK corpus: English multi-speaker corpus for CSTR voice cloning toolkit," *University of Edinburgh. The Centre for Speech Technology Research (CSTR)*, 2017.
- [80] I. Loshchilov and F. Hutter, "Decoupled weight decay regularization," *arXiv preprint arXiv:1711.05101*, 2017.
- [81] N. Zheng and X.-L. Zhang, "Phase-aware speech enhancement based on deep neural networks," *IEEE/ACM Transactions on Audio, Speech, and Language Processing*, vol. 27, no. 1, pp. 63–76, 2018.